Published online 28 February 2018

Nucleic Acids Research, 2018, Vol. 46, No. 9 ***4405–4416***
doi: 10.1093/nar/gky151

Comparative biochemical analysis of UHRF proteins reveals molecular mechanisms that uncouple UHRF2 from DNA methylation maintenance

Robert M. Vaughan[1], Bradley M. Dickson[1], Evan M. Cornett[1], Joseph S. Harrison[2,3], Brian Kuhlman[2,3] and Scott B. Rothbart[1,*]

[1]Center for Epigenetics, Van Andel Research Institute, Grand Rapids, MI 49503, USA, [2]Department of Biochemistry and Biophysics, University of North Carolina at Chapel Hill, NC 27599, USA and [3]Lineberger Comprehensive Cancer Center, University of North Carolina at Chapel Hill, NC 27599, USA

Received December 21, 2017; Revised February 13, 2018; Editorial Decision February 15, 2018; Accepted February 21, 2018

ABSTRACT

UHRF1 is a histone- and DNA-binding E3 ubiquitin ligase that functions with DNMT1 to maintain mammalian DNA methylation. UHRF1 facilitates DNMT1 recruitment to replicating chromatin through a coordinated mechanism involving histone and DNA recognition and histone ubiquitination. UHRF2 shares structural homology with UHRF1, but surprisingly lacks functional redundancy to facilitate DNA methylation maintenance. Molecular mechanisms uncoupling UHRF2 from DNA methylation maintenance are poorly defined. Through comprehensive and comparative biochemical analysis of recombinant human UHRF1 and UHRF2 reader and writer activities, we reveal conserved modes of histone PTM recognition but divergent DNA binding properties. While UHRF1 and UHRF2 diverge in their affinities toward hemi-methylated DNA, we surprisingly show that both hemi-methylated and hemi-hydroxymethylated DNA oligonucleotides stimulate UHRF2 ubiquitin ligase activity toward histone H3 peptide substrates. This is the first example of an E3 ligase allosterically regulated by DNA hydroxymethylation. However, UHRF2 is not a productive histone E3 ligase toward purified mononucleosomes, suggesting UHRF2 has an intra-domain architecture distinct from UHRF1 that is conformationally constrained when bound to chromatin. Collectively, our studies reveal that uncoupling of UHRF2 from the DNA methylation maintenance program is linked to differences in the molecular readout of chromatin signatures that connect UHRF1 to ubiquitination of histone H3.

INTRODUCTION

A major challenge of modern biology has been to determine how DNA-templated processes like transcription, replication and repair are temporally and spatially regulated in the context of chromatin. Histone post-translational modifications (PTMs) and DNA methylation have emerged as key regulators of chromatin accessibility, interaction, and signaling. Breakthroughs in our understanding of chromatin regulatory mechanisms have been made through the characterization of protein machineries that write, erase, and read these epigenetic marks. The faithful mitotic inheritance of DNA methylation patterns is essential for mammalian development and is well studied for its key roles in the stable transcriptional silencing of genes and transposable elements, genomic imprinting, and X-chromosome inactivation (1). DNA methylation patterns are established by *de novo* methyltransferases during early embryonic development and are maintained through somatic cell divisions by the maintenance methyltransferase DNMT1 (DNA methyltransferase 1), which has increased catalytic activity toward hemi-methylated DNA (He5mC) (2–4). The E3 ubiquitin ligase UHRF1 (ubiquitin-like, containing PHD and RING finger domains 1) is now appreciated as a key regulator of DNMT1-mediated DNA methylation maintenance. Genetic and biochemical studies revealed that UHRF1 plays a central role in DNMT1-directed DNA methylation maintenance during DNA replication (5,6). Deletion of *Uhrf1* (or *Np95*) in mice is embryonic lethal, and stem cells derived from *Uhrf1*$^{-/-}$ embryos (and also from human cells depleted of UHRF1) show a dramatic loss in DNA methylation, impaired maintenance of higher-order chromatin structure, and spurious transcription of otherwise silenced repetitive DNA elements (6–9).

The DNA methylation maintenance function of UHRF1 is dependent on its ability to bind chromatin, where it facilitates ubiquitination of histone H3 at lysines 18 and 23 (H3K18ub and H3K23ub, respectively), a proposed dock-

*To whom correspondence should be addressed. Tel: +1 616 234 5367; Email: scott.rothbart@vai.org

ing site for DNMT1 (10–13). UHRF1 has three domains that directly bind chromatin. The SRA (SET and RING-associated) domain of UHRF1 is a DNA-binding domain that recognizes 5-methylcytosine (5mC) in the context of hemi-methylated double-stranded CpG dinucleotides (14–16). UHRF1 also binds the unmodified N-terminus of histone H3 through a plant homeodomain (PHD) finger (17,18) and di- and tri-methylated lysine 9 on histone H3 (H3K9me2/me3) through an aromatic cage in the first subdomain of its tandem Tudor (19,20). Our studies showed that multivalent recognition of histone H3 by the UHRF1 TTD-PHD is required for its DNA methylation maintenance function in human cancer cells (21). We and others also defined a positive allosteric relationship between the histone- and DNA-binding activities of UHRF1 and showed that SRA binding to He5mC allosterically activates its ubiquitin ligase activity toward histone substrates (22–24).

The UHRF protein family has at least two *bona fide* members (25). UHRF2 is an E3 ubiquitin ligase that is also capable of SUMOylating proteins (26,27). However, there are few known substrates of UHRF2′s ubiquitin and SUMO ligase activities (28). UHRF2 is highly homologous to UHRF1 in sequence and structure (Supplementary Figure S1), but it does not appear to be functionally redundant in the maintenance of DNA methylation (22,29,30). The inability of UHRF2 to functionally compensate for UHRF1 is further demonstrated by the reduction of 5mC in *Uhrf1*-null mESCs, despite similar levels of *Uhrf1* and *Uhrf2* transcripts (DBTMEE, (31)). Recent studies reported that UHRF2 is a reader of 5hmC (32,33) and is required to maintain 5hmC levels in the brains of mice (34,35).

A mechanistic explanation for why UHRF2 is uncoupled from DNA methylation maintenance is lacking. Here, we compare and contrast the biochemical activities of UHRF1 and UHRF2 with modified histone peptides, DNA oligonucleotides, and purified mononucleosomes. We reveal similarities and differences in the reader and writer functions of these proteins. While UHRF1, but not UHRF2, has enhanced affinity for He5mC over unmodified DNA (UnDNA), He5mC stimulates the enzymatic activity of both UHRF proteins toward H3 peptide substrates. Surprisingly, the enzymatic activity of UHRF2, and to a lesser extent UHRF1, is stimulated by He5hmC, despite its inability to discriminate this mark from UnDNA or symmetrically modified (Sy5mC or Sy5hmC) DNA. Notably, we show that histone peptides, as substrates of UHRF1 and UHRF2 ubiquitin ligase activity, do not reveal differences that are apparent when using purified mononucleosomes as substrates. Our studies are consistent with a report showing that UHRF2 is unable to recruit DNMT1 to replicating chromatin (29), a finding we now propose is a result of its inability to ubiquitinate chromatinized histone substrates. Collectively, our studies reveal that the uncoupling of UHRF2 from the DNA methylation maintenance program is linked, at least in part, to differences in the molecular readout of chromatin signatures that connect UHRF1 to ubiquitination of histone H3. We suggest that differences in UHRF protein interactions with chromatin, presumably resulting from distinct intramolecular domain organization, contribute to a divergence in the writing of nucleosomal histone ubiquitination.

MATERIALS AND METHODS

Cell culture and plasmids

HeLa were originally purchased from ATCC and maintained in Dulbecco's Modified Eagle Medium (Life Technologies) supplemented with 10% FBS (Sigma) and 1% penicillin/streptomycin solution (Thermo), at 37°C with 5% CO_2. For bacterial expression, full length open reading frames of UHRF1 (1–793) and UHRF2 (1–802) were cloned by Gibson Assembly (NEB) into a modified pQE vector in frame with an N-terminal 6X histidine–maltose binding protein-tobacco etch virus cleavage site (6XHis-MBP-TEV). TTD-PHD (UHRF1: 125–364; UHRF2: 119–392) domains were cloned into pGEX-4T1 as N-terminal GST fusions. The expression construct for UBA1 was a gift from Dr Cynthia Wolberger (Addgene plasmid #34965). UBCH5A was a gift from Dr Rachel Klevit. The expression construct for TEV enzyme was a gift from Dr Jiyan Ma. The pSEB-N3F (N-terminal 3X-FLAG) used in chromatin association assays was a gift from Tong-Chuan He. UHRF2 ORFs were cloned into pSEB-N3F with HindIII and MluI restriction sites.

Chromatin association assays

HeLa cells were transfected with XtremeGene HP (Roche) at a 3:1 ratio with plasmid DNA in 60 mm dishes. After 48 h, cells were harvested by scraping into cold 1× PBS pH 7.6, pelleted at 1000 g for 5 min, and resuspended in 120 μl cold CSK buffer (10 mM PIPES pH 7.0, 300 mM sucrose, 100 mM NaCl, 3 mM $MgCl_2$, 0.1% Triton X-100, protease inhibitors (Roche; 1 tablet per 20 ml)). Cells were kept on ice for 20 min. Total protein was quantified by Bradford Assay (BioRad), and 10% was combined with an equivalent volume of cold endonuclease-supplemented CSK (Pierce, 250 units/5 ml). Note that the concentration of the total fraction is now 0.5×. Remaining cell lysates were centrifuged at 1300 g for 5 min at 4°C. The supernatant (soluble fraction) was collected. The chromatin pellet was washed 1× in CSK buffer, and pelleted 1300 g for 5 min at 4°C. The supernatant was discarded and the chromatin pellet was solubilized in cold endonuclease-supplemented CSK buffer. Five microgram of total protein and volume equivalents of chromatin and soluble fractions were loaded for western blot analysis.

Recombinant protein production

Bacterial expression constructs were transformed into BL21(DE3) *Escherichia coli* and grown at 37°C in LB Lennox (Cassion) media in baffled flasks at 160 rpm. When cells reached an $OD_{600} = 0.8–1.0$, the temperature was lowered to 16°C, IPTG was added (0.5 mM), and cultures were incubated with shaking for 16 h. Bacteria were harvested by centrifugation and washed 1× with cold PBS pH 7.6. Pellets were either frozen at –80°C or resuspended in lysis buffer (His-tag: 50 mM Tris–HCl pH 8.0, 500 mM NaCl, 20 mM imidazole, 1 mM PMSF and 1 mM DTT; GST-tag:

1× D-PBS, 1 mM PMSF and 1 mM DTT). Lysis was performed on ice by addition of lysozyme (30 min), followed by five rounds of sonication (20 s of sonication, followed by 2 min on ice) at 40% amplitude with a micro-tip (Branson Digital 450). Lysates were cleared by centrifugation at 38 000 g for 30 min at 4°C. Purification was performed by batch technique as follows. Cleared lysates were mixed for 1 h at 4°C with His60 Superflow Resin (Clontech) or glutathione agarose (Pierce), 5 ml equilibrated in Buffer A (His-tag: 50 mM Tris–HCl pH 8.0, 500 mM NaCl, 20 mM imidazole; GST-tag: 1× D-PBS). Resin and bound protein were washed three times with 20 bed volumes of Buffer A, followed by elution in five bed volumes of Buffer B (His-tag: 25 mM HEPES pH 7.5, 100 mM NaCl, 250 mM imidazole; GST-tag: 1× D-PBS, 10 mM L-glutathione (Sigma)). Protein was either concentrated (Amicon Ultra 15, 30K MWCO) and injected onto a HiLoad 26/600 Superdex 200 (GE Healthcare) size-exclusion column equilibrated in SEC buffer (25 mM HEPES pH 7.5, 100 mM NaCl, 1 mM DTT) or dialyzed into TEV cleavage buffer (His-tag: 50 mM Tris–HCl pH 8.0, 1 mM DTT, 0.5 mM EDTA) with recombinant TEV protease (500 nM). Recombinant TEV protease was purified as described (36). Cleavage of the 6X His–MBP tag was performed overnight at 4°C, and the cleaved protein was isolated by size-exclusion chromatography. Fractions were checked for purity by SDS-PAGE and were pooled and concentrated. MBP- and GST-fusions were concentrated to >80 μM, and frozen at –80°C with 20% glycerol. Cleaved proteins were concentrated to >20 μM and snap frozen in small aliquots without glycerol.

Fluorescence polarization

For histone binding analysis, $H3_{(1–20)}$ peptides functionalized with N- or C-terminal 5-carboxyfluorescein (FAM) were synthesized by the High Throughput Peptide Synthesis and Array (HTPSA) Core Facility at UNC Chapel Hill. $H3_{(1–20)}$ peptides without FAM were used when monitoring the allosteric relationship between histone and DNA binding. For DNA binding analysis, complementary 12-bp DNA oligonucleotides with the following sequences [FAM-5′-CCATGXGCTGAC-3′ and 5′-GTCAGYGCATGG-3′ (UnDNA: X and Y are cytosine, He5mC: X is 5mC and Y is cytosine, Sy5mC: X and Y are 5mC, He5hmC: X is 5hmC and Y is cytosine, Sy5hmC: X and Y are 5hmC)] were resuspending in STE buffer (10 mM Tris–HCl pH 8.0, 100 mM NaCl, 1 mM EDTA). Equimolar amounts of sense and antisense oligos were combined and boiled in a water bath for 10 min, followed by slow cooling to room temperature to anneal. Oligo hybridization was checked by 20% PAGE followed by fluorescent imaging of the FAM-labeled duplex as well as by SYBR Gold (Thermo) staining of ssDNA. Oligos containing 5mC were synthesized by Eurofins Genomics, and those containing 5hmC were synthesized by the Keck Oligonucleotide Synthesis Facility (Yale University). For histone and DNA binding, proteins were characterized as either MBP- or GST-fusions. Proteins were titrated with 10 nM FAM-ligand in FP assay buffer (25 mM HEPES pH 7.5, 100 mM NaCl, 0.05% NP-40). For allosteric DNA binding analysis (Figure 3B), FP assay buffer included 150 mM NaCl. Assays in 25 μl volumes were performed at room temperature using black 384-well plates (Costar). Polarization (P) was measured on a Synergy Neo fluorescence microplate reader (Biotek). Fluorescence intensities were converted to anisotropy (A) with the equation $A = 2P/3\text{-}P$. Dissociation constants (K_d) were calculated by nonlinear regression analysis of anisotropy curves using a one-site binding model with Hill slope in GraphPad Prism. Error is reported as ± standard error of the mean (S.E.M.) from technical triplicate measurements. Presented data is representative of at least two biological replicates (new protein preps and DNA probes). We note some variability in measured binding constants across biological replicates. To control for this, each comparative DNA binding assay (UnDNA versus HeDNA versus SyDNA, and UHRF1 versus UHRF2) was performed in the same 384-well plate at the same time. The variability that we present is due to both biological and technical error, and compounded by difficulties in fitting K_d for low affinity interactions. A complete list of binding constants and associated errors from FP measurements are listed in Supplementary Table S3.

Ubiquitination assays

In vitro ubiquitination reactions were performed in 20 μl volumes for 20 min (unless otherwise indicated) at room temperature in ubiquitin assay buffer (50 mM HEPES pH 7.5, 66 mM NaCl, 8 mM ATP, 2.5 mM $MgCl_2$, 2.5 mM DTT). For all reactions (except Supplementary Figure S4), 6xHis-MBP tags were cleaved from UHRF1 and UHRF2. Reactions contained 1.5 μM E3, 50 nM E1 UBA1, 667 nM E2 UBCH5A, 5 μM TAMRA-ubiquitin (BioVision), and 13 μM $H3_{(1–32)}$K9me2 (C-terminal biotin), and 6.25 μM 12-bp duplex DNA oligo. The DNA oligos used in ubiquitination reactions have the same sequence and modifications as those used for fluorescence polarization, but were synthesized without FAM label. For *in vitro* ubiquitination of HeLa mononucleosomes, reactions were run in ubiquitin assay buffer containing 1.5 μM E3, 50 nM E1 UBA1, 667 nM E2 UBCH5A, 5 μM TAMRA-ubiquitin, and 0.5 μM HeLa mononucleosomes (Epicypher). In the comparative time course ubiquitination reaction of peptide (1 μM) and nucleosome (0.5 μM), moles of H3 were equal, and He5mC (6.25 μM) was only added to the peptide reactions. Reactions were quenched by the addition of 5× SDS loading buffer (250 mM Tris–HCl pH 6.8, 50% glycerol, 10% SDS, 6% beta-mercaptoethanol, 0.25% bromophenol blue) to a final concentration of 1×. Fresh beta-mercaptoethanol was added to the loading buffer to reduce E1-ub and E2-ub conjugates Ubiquitinated species were directly imaged in gel by Cy3 fluorescence (TAMRA-ubiquitin) on an Azure c400 imaging platform.

Nucleosome pulldowns

For *in vitro* nucleosome pulldowns, 5 μl of streptavidin-coated magnetic bead slurry (Pierce) per pulldown was equilibrated in pulldown buffer (25 mM HEPES pH 7.5, 100 mM NaCl, 0.5% BSA, 0.1% NP-40). Beads were incubated with 50 pmoles of H3K9me3-containing recombinant biotinylated nucleosomes (Epicypher) for 30 min at room temperature. Conjugated beads were washed twice for 5 min

in pulldown buffer. The indicated GST- or MBP-fusions (500 pmol) were incubated with conjugated beads overnight at 4°C. Beads were then washed three times for 5 min in pulldown buffer. Beads were boiled in 100 μl of 1× SDS loading buffer (50 mM Tris–HCl pH 6.8, 10% glycerol, 2% SDS, 1.2% beta-mercaptoethanol, 0.05% bromophenol blue), and 10 μl was loaded onto gels for western blot. Input lanes were loaded with 1% of the unbound protein fraction.

Histone peptide microarrays

Histone peptide synthesis (UNC HTPSA), fabrication of the microarray, and protein domain hybridization was performed as previously described (37,38). Briefly, arrays were blocked for 30 min in cold array hybridization buffer (1× PBS pH 7.6, 0.1% Tween-20, 5% BSA (OmniPur, Fraction V)) and GST-tagged proteins (1 μM) were hybridized to the microarray in a humidified chamber overnight at 4°C. Bound protein was labeled with α-GST primary and AlexaFluor 647-conjugated secondary antibodies (Supplementary Table S1). Microarrays were fluorescently imaged at 20 μm resolution on an Innoscan 1100AL microarray scanner (Innopsys). Image processing and data analysis was performed as previously described with ArrayNinja (39). For heat map construction, arrays were normalized to each other by IgG control spots and the brightest peptide was set equal to 1 (blue). Peptides were then ranked for UHRF1 TTD-PHD from high to low. Each unique peptide feature (see Supplementary Table S2 for a full list of peptide features spotted on the array) was spotted in triplicate two times per subarray, and values presented are the average of measured signals for these individual peptide spots.

Western blotting

After separation by SDS-PAGE, proteins were transferred to 0.45 μm PVDF membrane (Amersham Hybond P) using a semi-dry transfer apparatus (Hoefer) for 1.5 h at a constant current of 1 mA/cm^2. Membranes were blocked for 1 h at room temperature in blotting buffer (1× PBS pH 7.6, 0.1% Tween-20, 5% BSA). Primary antibodies (Supplementary Table S1) were hybridized overnight at 4°C with gentle agitation in blotting buffer. Membranes were then washed three times for 5 min in blotting buffer. HRP-conjugated secondary antibodies (GE Life Sciences) were hybridized at room temperature for 1 h in blotting buffer. Membranes were again washed three times for 5 min in blotting buffer and reacted with ECL Prime (GE Life Sciences). Blots were exposed to film and developed on a Kodak system.

RESULTS

UHRF1 and UHRF2 TTD-PHD have conserved reader activities towards the N-terminus of histone H3

The inability of endogenous UHRF2 to maintain cellular DNA methylation, in the absence of UHRF1, led us to hypothesize that differences in chromatin recognition and/or enzymatic activity contribute to a lack of UHRF2 functional redundancy with UHRF1. To test this hypothesis, we systematically compared and contrasted the reader and enzymatic activities of these proteins, including appreciated mechanisms of UHRF1 intramolecular crosstalk through multivalent histone and DNA engagement (22,23), as well as allosteric control of enzymatic activity by He5mC (24).

We first used histone peptide microarrays to query, in a high-throughput and parallel manner, the reader activities of the linked TTD-PHD domains of UHRF1 and UHRF2. The arrays displayed a synthetic library of over 250 unique modified histone peptides harboring single and combinations of PTMs (Supplementary Table S2), derived largely from mass spectrometry datasets (40–43). UHRF1 and UHRF2 TTD-PHD preferentially bound H3 peptides (Figure 1A and B), and both preferentially bound to H3K9me2- and H3K9me3-containing peptides (Figure 1B and C). Consistent with the known interaction of the UHRF1 PHD with the free N-terminus of H3 (17,18), PTMs on the first six residues of the H3 N-terminus perturbed UHRF1 histone binding on the arrays (Supplementary Figure S2). UHRF2 binding to arrays appeared less affected by N-terminal H3 PTMs.

To further query the individual TTD and PHD contributions to histone binding, we next generated predicted loss-of-function mutations in the UHRF2 TTD-PHD based on structural alignments with UHRF1 (Supplementary Figure S3, TTD*: tandem Tudor mutant, PHD*: plant homeodomain finger mutant). Both the TTD*-PHD and TTD-PHD* of UHRF1 and UHRF2 were again profiled by histone peptide microarray. Consistent with the TTD as the methyl-lysine reading unit (19,20), the TTD*-PHD from both UHRF1 and UHRF2 exhibited reduced reader activity toward H3K9 methylation (Figure 1C–E). Although subtle, UHRF2 TTD-PHD* maintained some binding to peptides containing H3K9me2/me3 while UHRF1 TTD-PHD* did not (Figure 1C and F–G), suggesting the interaction between UHRF2 and H3 may be less dependent on its PHD finger than UHRF1. Consistently, UHRF2 was more tolerant of asymmetric di-methylation of H3R2 (H3R2me2a) than UHRF1 (Figure 1C and Supplementary Figure S2B), a PTM known to inhibit H3 binding through the UHRF1 PHD (44,45).

We next used fluorescence polarization (FP) binding assays to quantitatively measure interactions between UHRF1 and UHRF2 TTD-PHD and H3 peptides. UHRF1 TTD-PHD had a ∼4-fold increase in affinity for $H3_{(1–20)}$K9me3 over the unmodified tail ($H3_{(1–20)}$K9un), while UHRF2 had a ∼7-fold increase in affinity for $H3_{(1–20)}$K9me3 over $H3_{(1–20)}$K9un (Figure 2A). As predicted from peptide array experiments, UHRF1 and UHRF2 TTD mutations demonstrated a lack of selectivity for H3K9me3 (Figure 2B). Consistent with UHRF1 and UHRF2 TTD-PHD binding the H3 tail in a multivalent manner (20,21), PHD mutations, or the addition of an N-terminal FAM to H3 tail peptides, greatly disrupted measured interactions of UHRF1 and UHRF2 (Figure 2). FP binding assays with full-length UHRF1 and UHRF2 verified that the H3K9me3 reader properties of the isolated TTD-PHD were conserved in full-length protein (Supplementary Figure S5A). Collectively, these results demonstrate that UHRF1 and UHRF2 have conserved histone binding properties through multivalent TTD-PHD engagement of H3K9me2/me3 peptides.

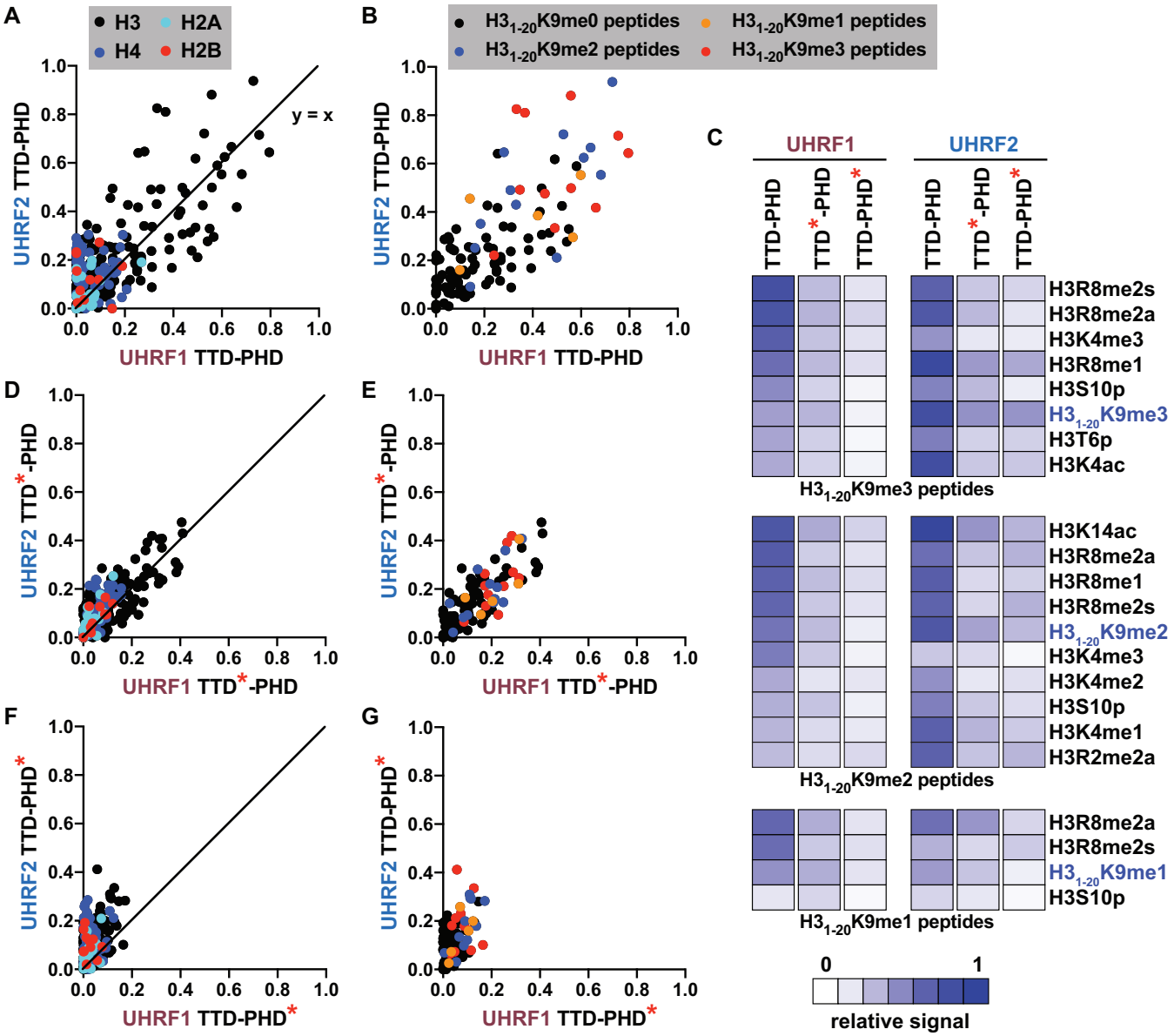

Figure 1. Functional requirements of histone PTM recognition are conserved between the UHRF1 and UHRF2 TTD-PHD. Scatter plots of normalized signal intensities from two subarrays hybridized with the indicated wild-type (**A**, **B**) and mutant (**D**–**G**) TTD-PHD domains of UHRF1 or UHRF2. Each spot represents average signal from a unique peptide feature (see Supplementary Table S2 for a full list of peptide features spotted on the array) and is color-coded by histone (A, D, F) or methylation state of $H3_{(1–20)}K9$ (B, E, G) as described in the key. Peptides are spotted in triplicate two times per subarray. Raw signal intensities for each peptide spot are normalized to the average IgG control signal on an individual subarray. (C) Heat maps showing the influence of neighboring PTMs on the indicated wild-type and mutant TTD-PHD interactions with arrayed $H3_{(1–20)}K9me3$ (top), $H3_{(1–20)}K9me2$ (middle) or $H3_{(1–20)}K9me1$ (bottom) peptides.

UHRF1, but not UHRF2, selectively binds He5mC

As the chromatin binding requirements of UHRF1 rely on both histone and DNA recognition (24), we next sought to compare the DNA binding properties of these two proteins. We again used FP binding assays to measure interactions between full-length UHRF1 and UHRF2 with 12-bp DNA oligonucleotides harboring a single, centrally-located CpG that was either unmodified (UnDNA), hemi-methylated (He5mC), or symmetrically methylated (Sy5mC). UHRF1 displayed a 9- to 32-fold increase (NaCl-dependent) in affinity for He5mC over UnDNA (Figure 3A, B left). However, UHRF2 had substantially reduced selectivity, in comparison to UHRF1, for either He5mC or Sy5mC over UnDNA (Figure 3A and B, right). We note a 2-fold affinity increase for He5mC over UnDNA for UHRF2 (Figure 3B, right), which may represent the error in fitting data without a clear upper plateau.

We and others previously reported a reciprocal positive allosteric relationship between the histone and DNA binding domains of UHRF1 (22–24). Consistent with our previous results, unlabeled $H3_{(1–20)}K9me3$ peptides enhanced the interaction of UHRF1 with both UnDNA and He5mC

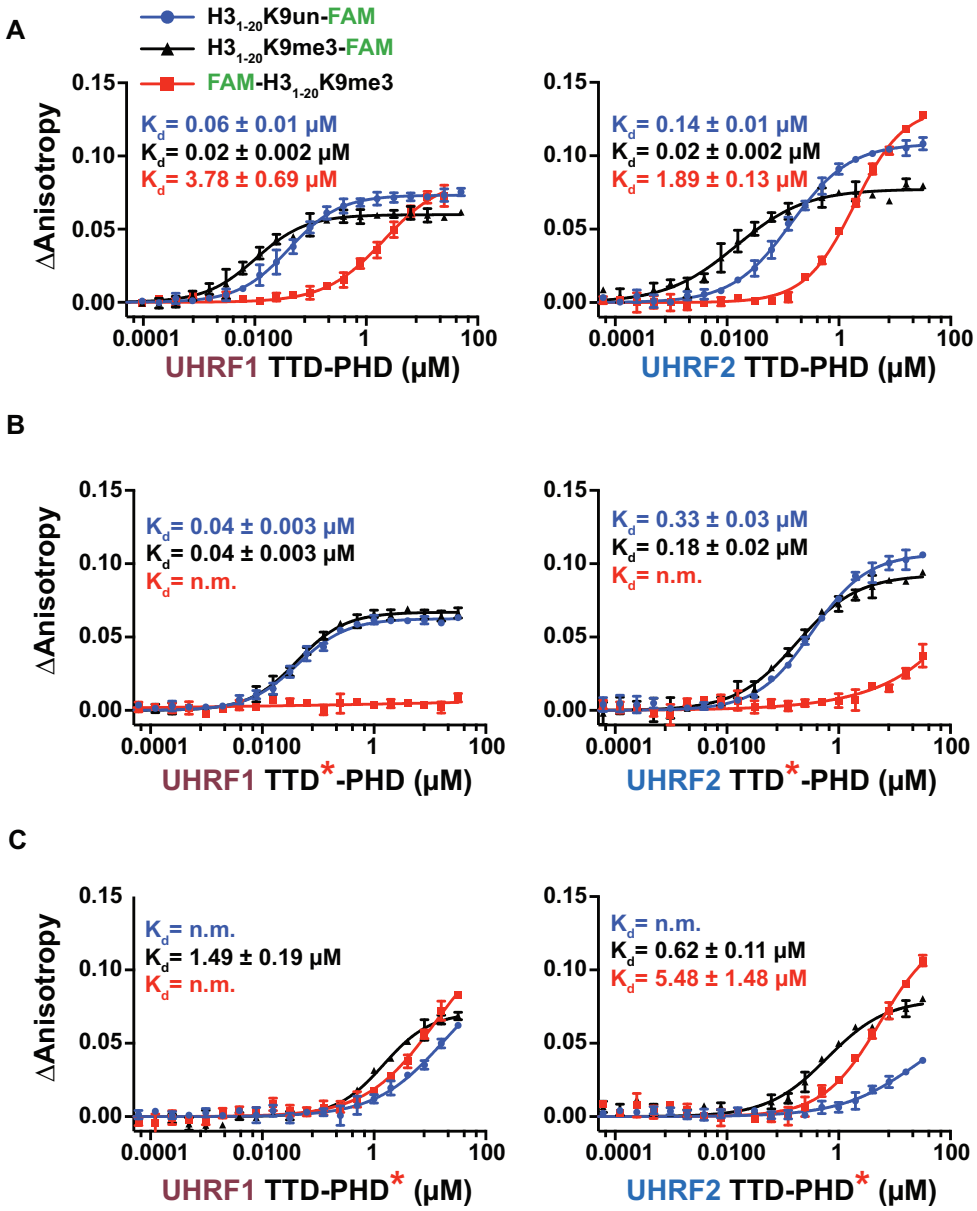

Figure 2. Multivalent histone engagement of UHRF proteins. Fluorescence polarization (FP) binding assays quantifying the interactions between wild-type (**A**) and mutant (**B, C**) TTD-PHD domains of UHRF1 or UHRF2 and the indicated FAM-labeled H3 peptides. Error bars represent s.e.m. from technical triplicate measurements. n.m., not measurable.

(Figure 3B, left). As observed for UHRF1, UHRF2 also maintains a positive allosteric relationship between histone and DNA binding (Figure 3B, right).

Although the reported affinity preference was modest (~3-fold preference for Sy5hmC over UnDNA), UHRF2 was previously reported to read 5hmC (33). We therefore sought to compare binding of UHRF1 and UHRF2 to 12-bp oligos modified with hemi-hydroxymethylated (He5hmC) and symmetrically hydroxymethylated (Sy5hmC) DNA (Figure 3C). Neither UHRF1, nor UHRF2, displayed increased affinity for DNA based on the hydroxymethyl state of a single CpG dinucleotide in our binding assay. Collectively, these results revealed that while UHRF1 and UHRF2 DNA binding activities were enhanced by histone engagement, UHRF2 lacked an increased affinity for He5mC in this sequence context. Furthermore, neither UHRF1 nor UHRF2 had a preference for He5hmC or Sy5hmC in this DNA sequence context.

UHRF1 and UHRF2 ubiquitin ligase activities are allosterically activated by hemi-modified DNA

As we previously showed that UHRF1 ubiquitin ligase activity toward H3 substrates was stimulated by He5mC oligonucleotides (24), we hypothesized that a lack of selective binding to He5mC, relative to UHRF1, would compromise the ubiquitin ligase activity of UHRF2. To test this hypothesis, we next performed comparative *in vitro*

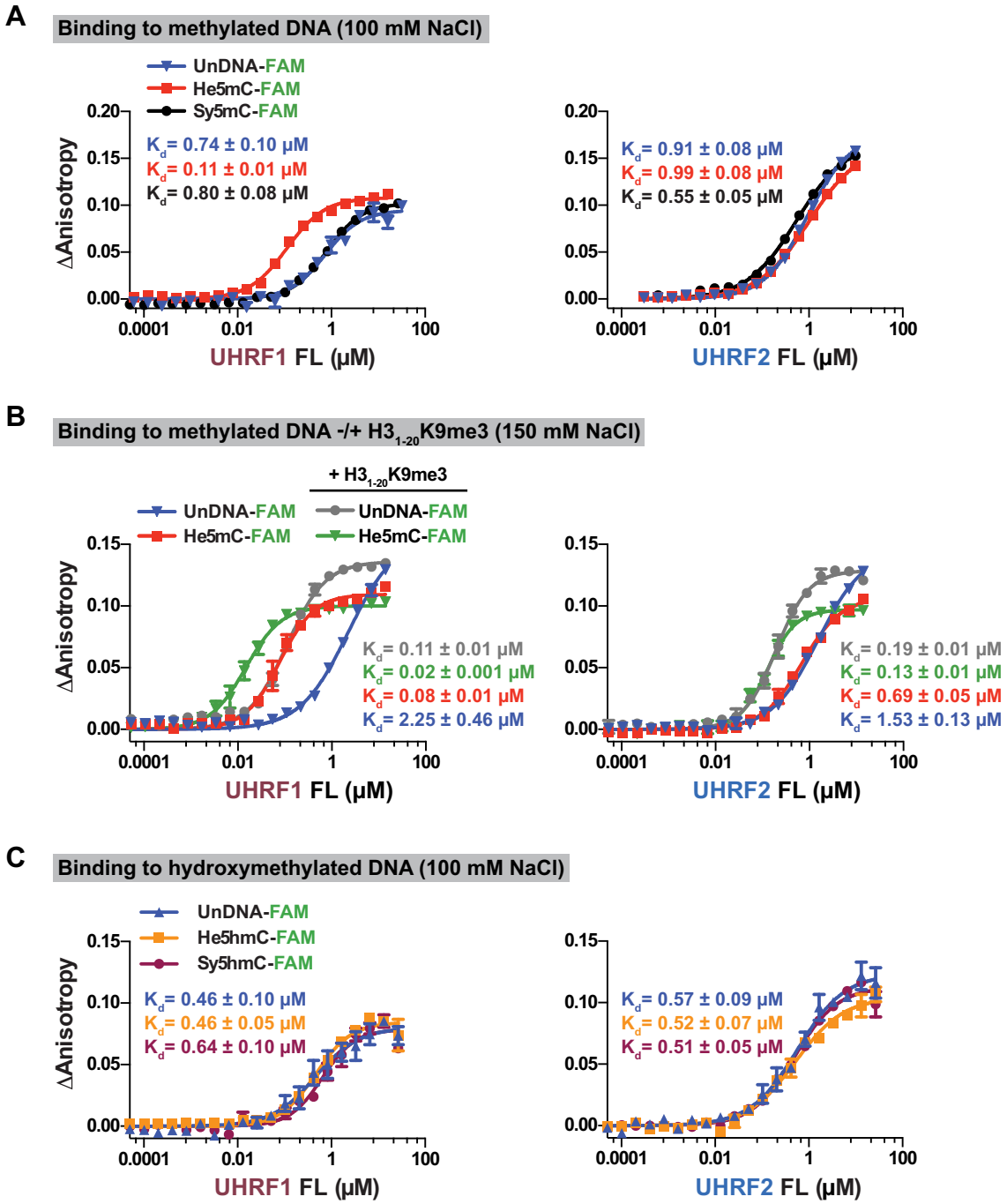

Figure 3. DNA binding analysis of full length UHRF1 and UHRF2 reveals divergence in He5mC reader activity. (**A–C**) FP binding assays quantifying the interactions between full-length UHRF1 (left) or UHRF2 (right) and the indicated FAM-labeled DNA oligonucleotides. For (**B**), FP measurements were made in the presence of a saturating concentration (13 μM) of $H3_{(1–20)}K9me3$. Error bars represent S.E.M. from technical triplicate measurements (A, B: 150 mM NaCl; C: 100 mM NaCl).

ubiquitination reactions for UHRF1 and UHRF2 with $H3_{(1–32)}K9me2$ peptide substrates in the absence or presence of saturating concentrations of modified DNA oligonucleotides (Figure 4A). Consistent with previous results, UHRF1 activity toward histone substrates and toward itself (auto-ubiquitination) was stimulated by He5mC. Surprisingly, UHRF2 enzymatic activity was also stimulated by He5mC, despite having substantially reduced selectivity for this mark over UnDNA, relative to UHRF1 (Figure 3A, B, and Figure 4A). In addition, He5hmC, but not Sy5hmC stimulated the enzymatic activity of UHRF2, and to a lesser extent UHRF1.

We next performed a time-course analysis of hemi-modified DNA activation of UHRF1 and UHRF2 ligase activities. UHRF1 and UHRF2 were indistinguishable in their ability to ubiquitinate themselves and $H3_{(1–32)}K9me2$

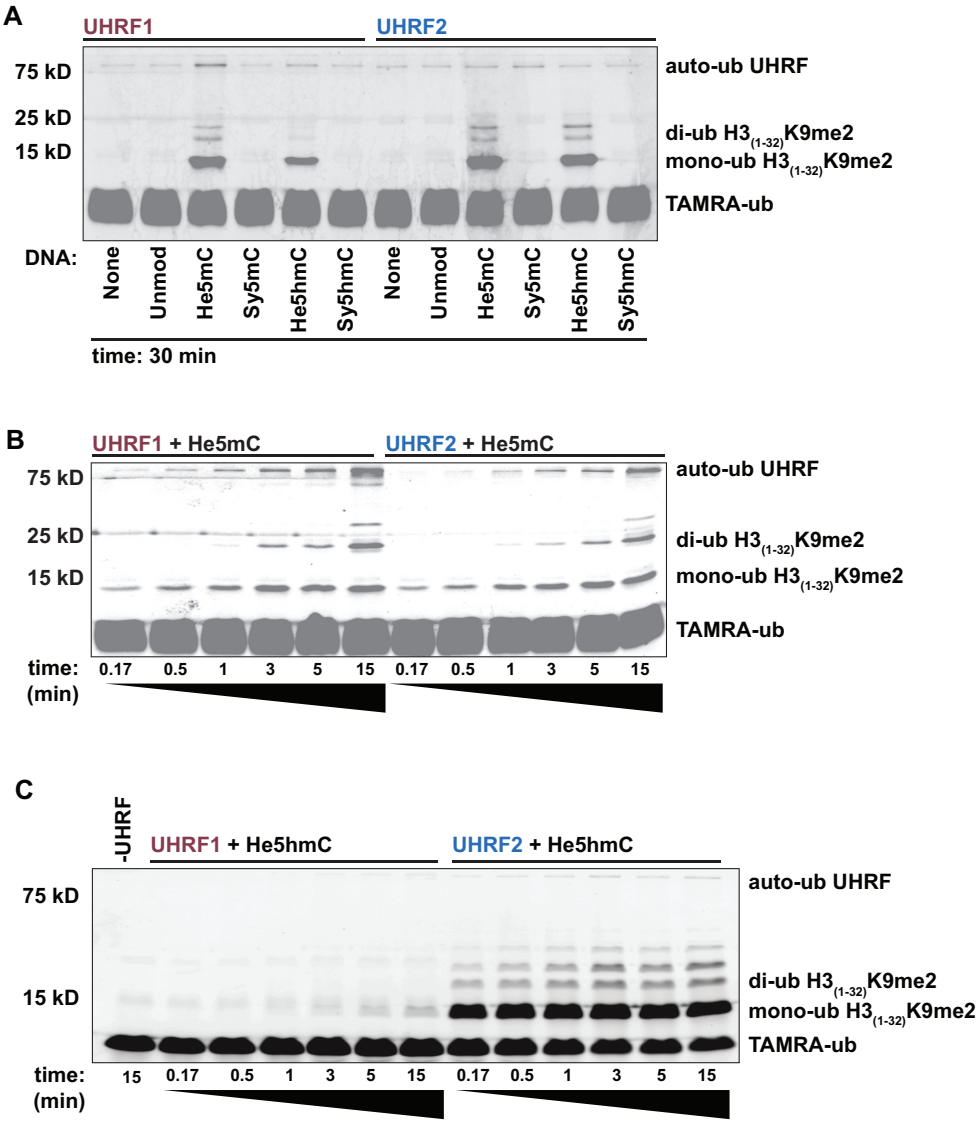

Figure 4. UHRF1 and UHRF2 E3 ligase activities are allosterically activated by hemi-modified DNA toward histone substrates. (**A**) *In vitro* ubiquitination of $H3_{(1–32)}$K9me2 by UHRF1 (left) or UHRF2 (right) in the absence or presence of a saturating concentration (6.25 μM) of the indicated DNA oligonucleotides. Time course *in vitro* ubiquitination of $H3_{(1–32)}$K9me2 by UHRF1 (left) or UHRF2 (right) in the presence of a saturating concentration (6.25 μM) of He5mC (**B**) or He5hmC (**C**).

peptide substrates in the presence of He5mC (Figure 4B). However, UHRF2 (but not UHRF1) enzymatic activity toward $H3_{(1–32)}$K9me2 peptide substrates was rapidly stimulated in the presence of He5hmC despite a lack of preference toward this mark for either protein (Figure 4C and Figure 3C). We note that the N-terminal MBP-tag slows the kinetics of the UHRF2 ubiquitination reaction (Supplementary Figure S4A), and we took advantage of this to capture the dynamics of He5hmC-stimulated UHRF2 ubiquitination (Supplementary Figure S4B, left). Introducing a loss-of-function mutation in the UHRF2 SRA (Supplementary Figure S3) disrupted He5hmC-dependent ubiquitin activity toward $H3_{(1–32)}$K9me2 peptide substrates (Supplementary Figure S4B). Collectively, these results demonstrated that UHRF1 and UHRF2 ubiquitin ligase activity is stimulated by He5mC, and that UHRF2 (but not UHRF1) activity is robustly stimulated by He5hmC and its interaction with the SRA domain. This is, to our knowledge, the first example of an E3 ubiquitin ligase allosterically regulated by DNA hydroxymethylation. Importantly, these results suggest that hemi-modified DNAs allosterically activate E3 ligase activity towards peptide substrates through a conformational change in UHRF proteins that is not discernable through FP binding measures.

UHRF2 ubiquitin ligase activity towards histones is restricted by chromatin

To evaluate how mutations in UHRF2 chromatin reading domains (TTD*, PHD*, and SRA*: G477D, Supplementary Figure S3) affected chromatin binding in cells, we performed chromatin association assays with FLAG-tagged UHRF2 (Figure 5A). In a behavior shared with

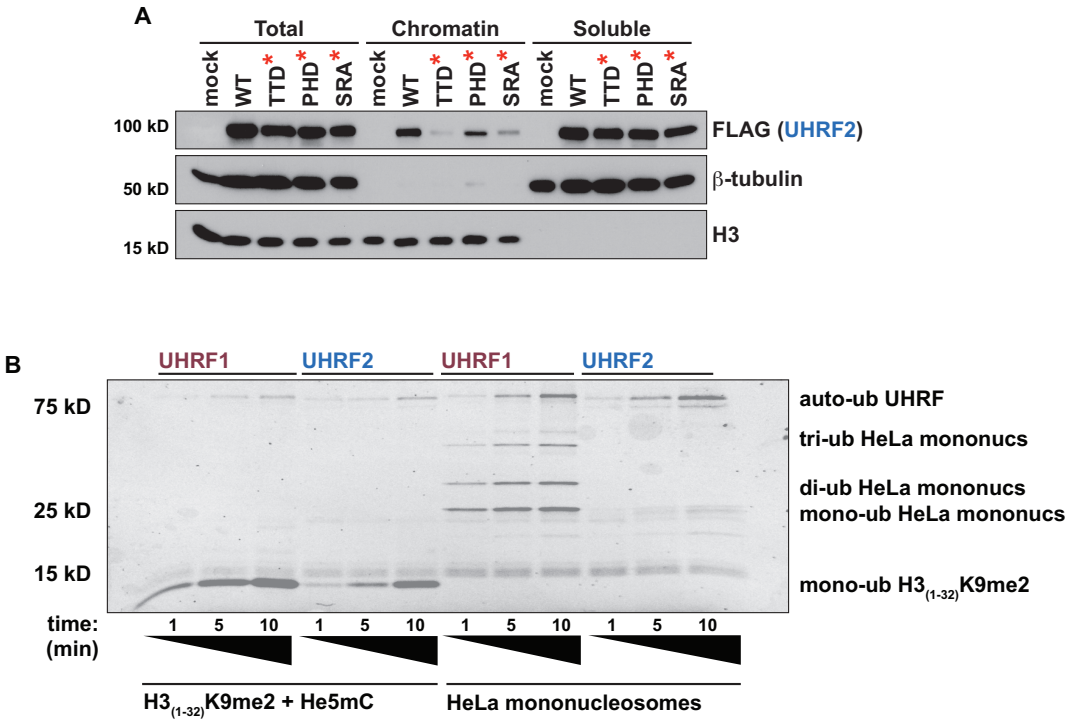

Figure 5. UHRF1 and UHRF2 diverge in their ability to ubiquitinate nucleosomal histones. (**A**) Chromatin association assays for FLAG-tagged UHRF2 (WT) or the indicated mutants from asynchronously growing HeLa cells. Mock treatment represents an empty vector control. (**B**) Comparative *in vitro* ubiquitination of $H3_{(1–32)}$K9me2 (left) and HeLa mononucleosomes (right) by UHRF1 and UHRF2. Moles of H3 are equivalent in these reactions.

UHRF1 (24), mutation of either histone- or DNA-binding domains reduced the amount of chromatin-bound UHRF2 in HeLa extracts. We next sought to compare E3 ligase activities of UHRF1 and UHRF2 on physiologic chromatin substrates using purified HeLa mononucleosome preparations. Surprisingly, UHRF2 was unable to ubiquitinate histones in the context of nucleosomes (Figure 5B, Supplementary Figure S5B). Auto-ubiquitination of UHRF2 in these assays confirmed the enzyme was active. We also performed a comparative ubiquitination reaction between UHRF1 and UHRF2 with both peptides and mononucleosomes where $H3_{(1–32)}$K9me2 was in two-fold molar excess over mononucleosomes to maintain equivalent moles of H3 (Figure 5B). Consistent with our initial findings (Figure 4B), UHRF1 and UHRF2 ubiquitin ligase activities toward $H3_{(1–32)}$K9me2 peptide substrates were similar (Figure 5B, left), but the activity difference toward histones was revealed when queried on nucleosomal substrates (Figure 5B, right). A possible explanation for the differences between UHRF1 and UHRF2 ligase activity in these assays was that UHRF2 binding to nucleosomes was weaker than UHRF1. However, pulldown assays would suggest the contrary, as more UHRF2 (TTD-PHD and full-length) pulled down with recombinant unmodified and H3K9me3-containing mononucleosomes than UHRF1 (Supplementary Figure S5C). Collectively, these findings show that while histone and DNA binding is required to target UHRF2 to bulk chromatin in cells, the assembly of UHRF2 on chromatin is likely distinct from UHRF1, resulting in a geometry unfavorable for histone ubiquitination. Consistent with this hypothesis, we were unable to stimulate UHRF2 enzymatic activity toward nucleosomal histone substrates by swapping the UHRF2 SRA with that of UHRF1 (Supplementary Figure S5B). Notably, a TTD-SRA swap was also not active as a nucleosomal histone E3 ligase, suggesting regions outside the chromatin binding unit also contribute to positioning UHRF1 in a conformation productive for nucleosomal histone ubiquitination. Both chimeric proteins retained auto-ubiquitination. As ubiquitination of H3K18 and H3K23 is required for the binding of DNMT1 to chromatin (13), our studies reveal a key biochemical difference between UHRF1 and UHRF2, at the level of nucleosomal histone ubiquitination, that restricts the ability of UHRF2 to functionally complement for UHRF1 as a regulator of DNA methylation maintenance.

DISCUSSION

Here we present a comprehensive biochemical comparison between two highly conserved E3 ubiquitin ligases, UHRF1 and UHRF2, and we reveal similarities and differences in chromatin recognition through histone and DNA binding, as well E3 ligase activities (summarized in Supplementary Table S4). This study sheds light on how multivalent chromatin engagement controls the enzymatic activity of UHRF proteins. We demonstrate that on H3 peptides, UHRF1 and UHRF2 E3 ligase activities are indistinguishably activated by He5mC. However, UHRF2 E3 ligase activity is robustly activated by He5hmC, while UHRF1 is not. This is, to our knowledge, the first allosteric function identified for 5hmC and suggests UHRF2 may play a role in the regulation and/or maintenance of this mark. Consistent with

this hypothesis, the enzymatic activity of TET2 was shown to be stimulated by UHRF2, and knockdown of UHRF2 resulted in accumulation of 5mC (30,32).

On nucleosome substrates, UHRF1 actively ubiquitinates histones, while UHRF2 does not. Our data show that the enzymatic differences between UHRF1 and UHRF2 are not due to histone substrate binding affinity differences (Supplementary Figure S5A, C). Rather, we suggest that when UHRF1 and UHRF2 engage histones and DNA in the context of a nucleosome, they adopt unique supertertiary structures (46). UHRF2 is constrained in a conformation that is incompatible with enzymatic activity toward histones, while UHRF1 is in a productive conformation. As UHRF2 is unable to deposit H3 ubiquitination, a proposed recruitment mechanism for DNMT1, UHRF2 is uncoupled from the maintenance of DNA methylation and unable to functionally compensate for UHRF1.

Our histone peptide microarray experiments revealed many subtle differences between UHRF1 and UHRF2 histone recognition, suggesting these H3 binding units may not be completely conserved in their mode of recognition. For peptides containing H3K9me2/me3, H3R2me2a and H3K4ac was tolerated by UHRF2, but not by UHRF1, while H3K4me3 was tolerated by UHRF1 but not for UHRF2 (Figure 1C). The differing influence of N-terminal modifications on UHRF1 and UHRF2 histone recognition suggests differences in the PHD domain and its interaction with the N-terminus of H3 (Supplementary Figure S2A, B). Indeed, in-cell validation of UHRF2 histone binding revealed that less UHRF2 was bound to chromatin with a loss-of-function mutation in the TTD than the PHD (Figure 5A). Interestingly, after filtering the microarray results for singly modified $H3_{(1–20)}$ peptides, we found that UHRF1 top hits included H3R8me1, H3R8me2s, H3K9me2, H3K18me3, and H3K14me3 (Supplementary Figure S2). The top hits for UHRF1 have not all been reported, and may represent new marks read by UHRF1. In contrast, UHRF2 top hits were clearly H3K9me3 and H3K9me2. Although we did not measure tighter binding for UHRF2 with H3 peptides than UHRF1 by FP (Figure 2A), this may be due to differences in the experimental setup of each assay. For FP assays, H3 tail peptides are in solution and free of any steric hindrance that may be provided by the nucleosome core particle or DNA. The microarray presents peptides immobilized on glass and may be more sterically representative of a histone tail protruding from the nucleosome core particle. Collectively, these data support that UHRF2 interaction with histones is more reliant on the TTD domain than the PHD domain. Comparative structural analysis of UHRF1 and UHRF2 TTD-PHD is likely to reveal subtle differences in the organization of these linked histone binding modules (there is no structure of UHRF2 TTD-PHD bound to H3).

UHRF1 and UHRF2 are the only mammalian proteins with an SRA domain. SRA domains have been extensively characterized as DNA binding domains in plants, and structural studies of SRA domains and various DNA probes consistently revealed a base flipped out of the DNA helix into a hydrophobic pocket of the SRA (14–16,47). To compare the DNA binding properties of UHRF1 and UHRF2, we first generated a mutation in the SRA domain of UHRF2 (SRA*: G477D) by introducing a negatively charged aspartic acid where the DNA backbone contacts the SRA domain (Supplementary Figure S3). The UHRF2 SRA* was informed by structural alignment with the UHRF1 SRA, and generation of the homologous UHRF1 G448D mutant known to disrupt DNA binding (24,48). We found that in addition to histone binding, DNA binding was required for UHRF2 chromatin association (Figure 5A). The co-requisites of histone and DNA binding for chromatin association revealed the multivalent nature of UHRF2, a behavior shared with UHRF1 (20,21,24). To comparatively evaluate the DNA binding properties of UHRF1 and UHRF2, we performed FP binding assays with modified DNA. UHRF1 demonstrated increased affinity toward He5mC DNA over UnDNA, whereas UHRF2 had minimal preference for methylated DNA of any state (Figure 3). In a behavior that is shared with UHRF1, the presence of H3K9me3 peptide increased affinity for DNA as measured by FP (Figure 3B). Although this positive allosteric mechanism is not structurally understood, we and others previously reported an interaction between the UHRF1 TTD-PHD and SRA-RING, and this interaction was modulated by DNA binding (23,24). It is important to note that this behavior was generally described for DNA, regardless of the methylation status. Understanding the coordinated binding of histone and DNA, for both UHRF1 and UHRF2, will require structural knowledge of the intra-domain organization of these proteins.

Existing data supporting UHRF proteins as specific readers of 5hmC is inconsistent (32,33,49). Crystal structures of the SRA domain of UHRF2 with He5mC and He5hmC have been solved, despite lacking increased affinity for either DNA probe over UnDNA, as measured by FP (33). To clarify whether UHRF1 or UHRF2 were readers of 5hmC, we measured binding to He5hmC and Sy5hmC DNA probes (Figure 3C). Neither UHRF1 nor UHRF2 showed increased affinity for 5hmC in either context by FP. Possible explanations for differences in our binding measures compared to others could be the composition of the DNA probe and the salt concentration used. Our probe is 12-bp in length with a single, centrally located CpG. Other studies have used longer probes with multiple 5hmC CpGs to enrich for UHRF2 (32). Measuring interactions with longer DNA probes with multiple 5hmC sites may reveal differences in stoichiometry rather than differences in affinity. Previous studies demonstrated salt concentration as a critical regulator of DNA binding constants (23,24), where lower salt resulted in tighter binding to DNA for UHRF1. We used both 100 mM and 150 mM NaCl for binding assays in this study, which must be considered when comparing our results to others. It is also possible that structural studies and binding assays with isolated domains do not accurately reflect the full-length protein behavior, as has been shown here for histone binding (Figure 2A and Supplementary Figure S5A), as well as by others for DNA binding (23,24).

Comparative ubiquitination assays for UHRF1 and UHRF2 were surprising in many ways. The first surprise was that both He5mC and He5hmC DNA probes activated the E3 ligase activity of UHRF1 toward H3K9me2 peptides (Figure 4A), although to a lesser degree for He5hmC. We

previously attributed the allosteric activation of UHRF1 by He5mC, at least in part, to an increased affinity for He5mC DNA (24). However, the activation of UHRF2 by He5mC and He5hmC is independent of increased affinity over UnDNA (Figures 3 and 4). The activation of UHRF1 and UHRF2 by any DNA that is hemi-modified suggests a conformational activation conditional upon binding of asymmetrically modified CpG dinucleotides (Figure 4). Our data introduce a new paradigm to the field. In the strict definition of mark discrimination through affinity measurements, we would not call the UHRF2 SRA domain a 5hmC reader. However, UHRF2 is clearly 'reading' 5hmC-modified DNA in a unique way that results in allosteric activation of its E3 ligase activity. We propose that the definition of an epigenetic 'reader' be refined to not only include proteins that measure increased affinity for a specific modification state, but also for proteins whose enzymatic activity is modulated by the mark they are reading. Future studies are needed to understand the molecular basis of hemi-modified DNA-dependent activation of UHRF1 and UHRF2 E3 ligase activity.

As histone peptides and DNA probes are not physically linked as they would be presented in a nucleosome, they represent a *trans* model. The *trans* nature of our ubiquitination assays provided no conformational restraint to the geometries of UHRF1 and UHRF2, and resulted in no significant differences in E3 ligase activity by He5mC activation. By performing ubiquitination reactions on purified mononucleosomes, we introduced physical constraints to UHRF1 and UHRF2, with histone and DNA presented in a *cis* fashion (Figure 5B and Supplementary Figure S5B). With conformational constraint imposed on UHRF1 and UHRF2 by engagement of the nucleosome, only UHRF1 was a productive E3 ligase. These data support a hypothesis that intramolecular geometries of UHRF1 and UHRF2, as conferred by divergence of their intra-domain architecture, are key differences that govern allosteric control of E3 ligase activity. Alternatively, differences in He5mC specificities between UHRF1 and UHRF2 may be borne out in the context of the nucleosome that are otherwise missed studying activities with free peptides and DNA oligonucleotides. Future studies evaluating the interactions and activities of UHRF1 and UHRF2 with nucleosomes will reveal molecular details regulating the divergent substrate specificities of these two enigmatic proteins.

DATA AVAILABILITY

ArrayNinja software for the fabrication and analysis of microarray experiments is freely available (http://research.vai.org/Tools/arrayninja/). All plasmids are available upon request.

SUPPLEMENTARY DATA

Supplementary Data are available at NAR Online.

ACKNOWLEDGEMENTS

We thank Amy Nelson for administrative support and members of the Rothbart Lab for insightful comments and critiques of this study. We also thank Krzysztof Krajewski and the UNC HTPSA for synthesizing peptides used in this study.

FUNDING

National Institutes of Health [GM124736 to S.B.R.]; Van Andel Research Institute [to S.B.R.]; Van Andel Institute Graduate School [to R.M.V.]. Funding for open access charge: National Institutes of Health [GM124736].
Conflict of interest statement. None declared.

REFERENCES

1. Smith,Z.D. and Meissner,A. (2013) DNA methylation: roles in mammalian development. *Nat. Rev. Genet.*, **14**, 204–220.
2. Okano,M., Xie,S. and Li,E. (1998) Cloning and characterization of a family of novel mammalian DNA (cytosine-5) methyltransferases. *Nat. Genet.*, **19**, 219–220.
3. Pradhan,S., Bacolla,A., Wells,R.D. and Roberts,R.J. (1999) Recombinant human DNA (cytosine-5) methyltransferase. I. Expression, purification, and comparison of de novo and maintenance methylation. *J. Biol. Chem.*, **274**, 33002–33010.
4. Hermann,A., Gowher,H. and Jeltsch,A. (2004) Biochemistry and biology of mammalian DNA methyltransferases. *Cell. Mol. Life Sci. CMLS*, **61**, 2571–2587.
5. Bostick,M., Kim,J.K., Estève,P.-O., Clark,A., Pradhan,S. and Jacobsen,S.E. (2007) UHRF1 plays a role in maintaining DNA methylation in mammalian cells. *Science*, **317**, 1760–1764.
6. Sharif,J., Muto,M., Takebayashi,S., Suetake,I., Iwamatsu,A., Endo,T.A., Shinga,J., Mizutani-Koseki,Y., Toyoda,T., Okamura,K. *et al.* (2007) The SRA protein Np95 mediates epigenetic inheritance by recruiting Dnmt1 to methylated DNA. *Nature*, **450**, 908–912.
7. Muto,M., Kanari,Y., Kubo,E., Takabe,T., Kurihara,T., Fujimori,A. and Tatsumi,K. (2002) Targeted disruption of Np95 gene renders murine embryonic stem cells hypersensitive to DNA damaging agents and DNA replication blocks. *J. Biol. Chem.*, **277**, 34549–34555.
8. Papait,R., Pistore,C., Negri,D., Pecoraro,D., Cantarini,L. and Bonapace,I.M. (2007) Np95 is implicated in pericentromeric heterochromatin replication and in major satellite silencing. *Mol. Biol. Cell*, **18**, 1098–1106.
9. Sharif,J., Endo,T.A., Nakayama,M., Karimi,M.M., Shimada,M., Katsuyama,K., Goyal,P., Brind'Amour,J., Sun,M.-A., Sun,Z. *et al.* (2016) Activation of endogenous retroviruses in Dnmt1−/− ESCs involves disruption of SETDB1-mediated repression by NP95 binding to hemimethylated DNA. *Cell Stem Cell*, **19**, 81–94.
10. Rothbart,S.B., Krajewski,K., Nady,N., Tempel,W., Xue,S., Badeaux,A.I., Barsyte-Lovejoy,D., Martinez,J.Y., Bedford,M.T., Fuchs,S.M. *et al.* (2012) Association of UHRF1 with methylated H3K9 directs the maintenance of DNA methylation. *Nat. Struct. Mol. Biol.*, **19**, 1155–1160.
11. Nishiyama,A., Yamaguchi,L., Sharif,J., Johmura,Y., Kawamura,T., Nakanishi,K., Shimamura,S., Arita,K., Kodama,T., Ishikawa,F. *et al.* (2013) Uhrf1-dependent H3K23 ubiquitylation couples maintenance DNA methylation and replication. *Nature*, **502**, 249–253.
12. Qin,W., Wolf,P., Liu,N., Link,S., Smets,M., La Mastra,F., Forné,I., Pichler,G., Hörl,D., Fellinger,K. *et al.* (2015) DNA methylation requires a DNMT1 ubiquitin interacting motif (UIM) and histone ubiquitination. *Cell Res.*, **25**, 911–929.
13. Ishiyama,S., Nishiyama,A., Saeki,Y., Moritsugu,K., Morimoto,D., Yamaguchi,L., Arai,N., Matsumura,R., Kawakami,T., Mishima,Y. *et al.* (2017) Structure of the Dnmt1 reader module complexed with a unique two-mono-ubiquitin mark on histone H3 reveals the basis for DNA methylation maintenance. *Mol. Cell*, **68**, 350–360.
14. Avvakumov,G.V., Walker,J.R., Xue,S., Li,Y., Duan,S., Bronner,C., Arrowsmith,C.H. and Dhe-Paganon,S. (2008) Structural basis for recognition of hemi-methylated DNA by the SRA domain of human UHRF1. *Nature*, **455**, 822–825.
15. Hashimoto,H., Horton,J.R., Zhang,X., Bostick,M., Jacobsen,S.E. and Cheng,X. (2008) The SRA domain of UHRF1 flips 5-methylcytosine out of the DNA helix. *Nature*, **455**, 826–829.

16. Qian,C., Li,S., Jakoncic,J., Zeng,L., Walsh,M.J. and Zhou,M.-M. (2008) Structure and hemimethylated CpG binding of the SRA domain from human UHRF1. *J. Biol. Chem.*, **283**, 34490–34494.
17. Hu,L., Li,Z., Wang,P., Lin,Y. and Xu,Y. (2011) Crystal structure of PHD domain of UHRF1 and insights into recognition of unmodified histone H3 arginine residue 2. *Cell Res.*, **21**, 1374–1378.
18. Lallous,N., Legrand,P., McEwen,A.G., Ramón-Maiques,S., Samama,J.-P. and Birck,C. (2011) The PHD finger of human UHRF1 reveals a new subgroup of unmethylated histone H3 tail readers. *PLoS One*, **6**, e27599.
19. Nady,N., Lemak,A., Walker,J.R., Avvakumov,G.V., Kareta,M.S., Achour,M., Xue,S., Duan,S., Allali-Hassani,A., Zuo,X. *et al.* (2011) Recognition of Multivalent Histone States Associated with Heterochromatin by UHRF1 Protein. *J. Biol. Chem.*, **286**, 24300–24311.
20. Arita,K., Isogai,S., Oda,T., Unoki,M., Sugita,K., Sekiyama,N., Kuwata,K., Hamamoto,R., Tochio,H., Sato,M. *et al.* (2012) Recognition of modification status on a histone H3 tail by linked histone reader modules of the epigenetic regulator UHRF1. *Proc. Natl. Acad. Sci. U.S.A.*, **109**, 12950–12955.
21. Rothbart,S.B., Dickson,B.M., Ong,M.S., Krajewski,K., Houliston,S., Kireev,D.B., Arrowsmith,C.H. and Strahl,B.D. (2013) Multivalent histone engagement by the linked tandem Tudor and PHD domains of UHRF1 is required for the epigenetic inheritance of DNA methylation. *Genes Dev.*, **27**, 1288–1298.
22. Pichler,G., Wolf,P., Schmidt,C.S., Meilinger,D., Schneider,K., Frauer,C., Fellinger,K., Rottach,A. and Leonhardt,H. (2011) Cooperative DNA and histone binding by Uhrf2 links the two major repressive epigenetic pathways. *J. Cell. Biochem.*, **112**, 2585–2593.
23. Fang,J., Cheng,J., Wang,J., Zhang,Q., Liu,M., Gong,R., Wang,P., Zhang,X., Feng,Y., Lan,W. *et al.* (2016) Hemi-methylated DNA opens a closed conformation of UHRF1 to facilitate its histone recognition. *Nat. Commun.*, **7**, 11197.
24. Harrison,J.S., Cornett,E.M., Goldfarb,D., DaRosa,P.A., Li,Z.M., Yan,F., Dickson,B.M., Guo,A.H., Cantu,D.V., Kaustov,L. *et al.* (2016) Hemi-methylated DNA regulates DNA methylation inheritance through allosteric activation of H3 ubiquitylation by UHRF1. *eLife*, **5**, e17101.
25. Bronner,C., Achour,M., Arima,Y., Chataigneau,T., Saya,H. and Schini-Kerth,V.B. (2007) The UHRF family: Oncogenes that are drugable targets for cancer therapy in the near future? *Pharmacol. Ther.*, **115**, 419–434.
26. Mori,T., Li,Y., Hata,H. and Kochi,H. (2004) NIRF is a ubiquitin ligase that is capable of ubiquitinating PCNP, a PEST-containing nuclear protein. *FEBS Lett.*, **557**, 209–214.
27. Oh,Y. and Chung,K.C. (2013) UHRF2, a ubiquitin E3 ligase, acts as a small ubiquitin-like modifier E3 ligase for zinc finger protein 131. *J. Biol. Chem.*, **288**, 9102–9111.
28. Karg,E., Smets,M., Ryan,J., Forné,I., Qin,W., Mulholland,C.B., Kalideris,G., Imhof,A., Bultmann,S. and Leonhardt,H. (2017) Ubiquitome analysis reveals PCNA-associated factor 15 (PAF15) as a specific ubiquitination target of UHRF1 in embryonic stem cells. *J. Mol. Biol.*, **429**, 3814–3824.
29. Zhang,J., Gao,Q., Li,P., Liu,X., Jia,Y., Wu,W., Li,J., Dong,S., Koseki,H. and Wong,J. (2011) S phase-dependent interaction with DNMT1 dictates the role of UHRF1 but not UHRF2 in DNA methylation maintenance. *Cell Res.*, **21**, 1723–1739.
30. Jia,Y., Li,P., Fang,L., Zhu,H., Xu,L., Cheng,H., Zhang,J., Li,F., Feng,Y., Li,Y. *et al.* (2016) Negative regulation of DNMT3A de novo DNA methylation by frequently overexpressed UHRF family proteins as a mechanism for widespread DNA hypomethylation in cancer. *Cell Discov.*, **2**, 16007.
31. Park,S.-J., Shirahige,K., Ohsugi,M. and Nakai,K. (2015) DBTMEE: a database of transcriptome in mouse early embryos. *Nucleic Acids Res.*, **43**, D771–D776.
32. Spruijt,C.G., Gnerlich,F., Smits,A.H., Pfaffeneder,T., Jansen,P.W.T.C., Bauer,C., Münzel,M., Wagner,M., Müller,M., Khan,F. *et al.* (2013) Dynamic readers for 5-(hydroxy)Methylcytosine and its oxidized derivatives. *Cell*, **152**, 1146–1159.
33. Zhou,T., Xiong,J., Wang,M., Yang,N., Wong,J., Zhu,B. and Xu,R.-M. (2014) Structural basis for hydroxymethylcytosine recognition by the SRA domain of UHRF2. *Mol. Cell*, **54**, 879–886.
34. Chen,R., Zhang,Q., Duan,X., York,P., Chen,G.-D., Yin,P., Zhu,H., Xu,M., Chen,P., Wu,Q. *et al.* (2017) The 5-hydroxymethylcytosine (5hmC) reader UHRF2 is required for normal levels of 5hmC in mouse adult brain and spatial learning and memory. *J. Biol. Chem.*, **292**, 4533–4543.
35. Liu,Y., Zhang,B., Meng,X., Korn,M.J., Parent,J.M., Lu,L.-Y. and Yu,X. (2017) UHRF2 regulates local 5-methylcytosine and suppresses spontaneous seizures. *Epigenetics*, **12**, 551–560.
36. Kapust,R.B., Tözsér,J., Fox,J.D., Anderson,D.E., Cherry,S., Copeland,T.D. and Waugh,D.S. (2001) Tobacco etch virus protease: mechanism of autolysis and rational design of stable mutants with wild-type catalytic proficiency. *Protein Eng. Des. Sel.*, **14**, 993–1000.
37. Rothbart,S.B., Krajewski,K., Strahl,B.D. and Fuchs,S.M. (2012) Peptide microarrays to interrogate the 'histone code'. *Methods Enzymol.*, **512**, 107–135.
38. Cornett,E.M., Dickson,B.M., Vaughan,R.M., Krishnan,S., Trievel,R.C., Strahl,B.D. and Rothbart,S.B. (2016) Substrate specificity profiling of histone-modifying enzymes by peptide microarray. *Methods Enzymol.*, **574**, 31–52.
39. Dickson,B.M., Cornett,E.M., Ramjan,Z. and Rothbart,S.B. (2016) ArrayNinja: an open source platform for unified planning and analysis of microarray experiments. *Methods Enzymol.*, **574**, 53–77.
40. Pesavento,J.J., Yang,H., Kelleher,N.L. and Mizzen,C.A. (2008) Certain and progressive methylation of histone H4 at lysine 20 during the cell cycle. *Mol. Cell. Biol.*, **28**, 468–486.
41. Sidoli,S., Cheng,L. and Jensen,O.N. (2012) Proteomics in chromatin biology and epigenetics: elucidation of post-translational modifications of histone proteins by mass spectrometry. *J. Proteomics*, **75**, 3419–3433.
42. Young,N.L., DiMaggio,P.A., Plazas-Mayorca,M.D., Baliban,R.C., Floudas,C.A. and Garcia,B.A. (2009) High throughput characterization of combinatorial histone codes. *Mol. Cell. Proteomics MCP*, **8**, 2266–2284.
43. Young,N.L., Dimaggio,P.A. and Garcia,B.A. (2010) The significance, development and progress of high-throughput combinatorial histone code analysis. *Cell. Mol. Life Sci. CMLS*, **67**, 3983–4000.
44. Rajakumara,E., Wang,Z., Ma,H., Hu,L., Chen,H., Lin,Y., Guo,R., Wu,F., Li,H., Lan,F. *et al.* (2011) PHD finger recognition of unmodified histone H3R2 links UHRF1 to regulation of euchromatic gene expression. *Mol. Cell*, **43**, 275–284.
45. Veland,N., Hardikar,S., Zhong,Y., Gayatri,S., Dan,J., Strahl,B.D., Rothbart,S.B., Bedford,M.T. and Chen,T. (2017) The arginine methyltransferase PRMT6 regulates DNA methylation and contributes to global DNA hypomethylation in cancer. *Cell Rep.*, **21**, 3390–3397.
46. Tompa,P. (2012) On the supertertiary structure of proteins. *Nat. Chem. Biol.*, **8**, 597–600.
47. Arita,K., Ariyoshi,M., Tochio,H., Nakamura,Y. and Shirakawa,M. (2008) Recognition of hemi-methylated DNA by the SRA protein UHRF1 by a base-flipping mechanism. *Nature*, **455**, 818–821.
48. Achour,M., Mousli,M., Alhosin,M., Ibrahim,A., Peluso,J., Muller,C.D., Schini-Kerth,V.B., Hamiche,A., Dhe-Paganon,S. and Bronner,C. (2013) Epigallocatechin-3-gallate up-regulates tumor suppressor gene expression via a reactive oxygen species-dependent down-regulation of UHRF1. *Biochem. Biophys. Res. Commun.*, **430**, 208–212.
49. Frauer,C., Hoffmann,T., Bultmann,S., Casa,V., Cardoso,M.C., Antes,I. and Leonhardt,H. (2011) Recognition of 5-hydroxymethylcytosine by the Uhrf1 SRA domain. *PLoS One*, **6**, e21306.